# Polyoxymethylene/Ethylene Butylacrylate Copolymer/ Ethylene-Methyl Acrylate-Glycidyl Methacrylate Ternary Blends

**Wenqing Yang,[1] Xuan-Lun Wang,[1] Jianfeng Li,[2] Xingru Yan,[3] Shengsong Ge,[2] Sruthi Tadakamalla,[4] Zhanhu Guo[3]**

[1]*College of Materials Science and Engineering, Chongqing University of Technology, Chongqing, 400054, China*
[2]*Integrated Composites Laboratory (ICL), Department of Chemical & Biomolecular Engineering, University of Tennessee, Knoxville, Tennessee, 37997*
[3]*College of Chemical and Environmental Engineering, Shandong University of Science and Technology, Qingdao, 266590, People's Republic of China*
[4]*Engineered Multifunctional Composites (EMC) Nanotechnology LLC, Knoxville, Tennessee, 37934*

**Blends of compatibilized polyoxymethylene (POM)/ethylene butylacrylate copolymer (EBA)/ethylene-methyl acrylate-glycidyl methacrylate copolymer (EMA-GMA) and uncompatibilized POM/EBA were investigated. The notched impact strength of the compatibilized blends was higher than that of their uncompatibilized counterparts. The toughness of the POM blends was improved obviously with relatively low loading of EBA. Fourier transform infrared spectroscopy (FTIR) spectra of EMA-GMA, pure POM, and POM/EBA/EMA-GMA blends indicated that epoxy groups of EMA-GMA reacted with terminal hydroxyl groups of POM molecular chains. The glass-transition temperature ($T_g$) values of the POM matrix and the EBA phase were observed shifted to each other in the presence of EMA-GMA compatibilizer indicating that the compatibilized blends had better compatibility than their uncompatibilized counterparts. With the addition of EBA to POM, both the compatibilized and uncompatibilized blends showed higher onset degradation temperature ($T_d$) than that of pure POM and the $T_d$ values of the compatibilized blends were higher than those of their uncompatibilized counterparts. The scanning electron microscopy showed better EBA particles distribution state in the compatibilized system than in the uncompatibilized one. The compatibilized blend with an obvious rougher impact fracture surface indicated the ductile fracture mode. POLYM. ENG. SCI., 00:000–000, 2017.** 

## INTRODUCTION

Modifying polymers is an easier and cheaper way to obtain desired materials rather than synthesizing new ones [1–10]. Blending is an effective and convenient method to modify polymers [11–15]. Many polymers have been modified by blending, like polypropylene (PP) [16], polyamide [17, 18], polyethylene terephthalate (PET) [19, 20], polycarbonate (PC) [21], polyvinyl chloride [22], and so forth. POM, an excellent engineering plastic, has been widely used in irrigation, plumbing, molded door handles, pump impellers, tea kettles, plumbing fixtures, and shoe heels since its commercialization in 1959 due to its good thread strength, creep resistance, and torque retention [23]. However, POM is sensitive to crack, and its notched impact strength is relatively low that limits its applications. Thus, improving POM impact strength is a paramount necessity to enlarge its scope of utilization, including robots [24] and unmanned driving vehicles [25], as it is a unique timely moment for embedding intelligence in applications [26].

Thermoplastic polyurethane (TPU), a toughening agent with excellent properties, has been widely used to toughen plastics like PP [27], poly(butylene terephthalate) [28], polylactic acid (PLA) [29, 30], poly(methyl methacrylate) [31], and especially polyoxymethylene (POM) [32–40]. TPU has been proved to be an effective toughening agent to POM as ether oxygen from POM and urethane group from TPU can form hydrogen bonding to enhance the interfacial adhesion between POM matrix and TPU particles [41]. However, TPU is very expensive, therefore other materials have been applied to toughen POM. For example, dynamically vulcanized ethylene propylene diene terpolymer [42], ethylene octene copolymer elastomers (EOC) [43], dynamically vulcanized EOC elastomers [44], acrylate elastomer [45], poly(ethylene oxide) [46], polytetrafluoroethylene fibers [47] have been reported to toughen POM. Ethylene butylacrylate copolymer (EBA) is an excellent toughening agent with high molecular polarity and good compatibility with many polymers. EBA has been used to toughen polyamide 6 [48] and PLA [49], but has not been used as a toughening agent for POM yet. A compatibilizer is a very important component to prepare polymer blends [50–54] as it can enhance the interfacial adhesion between the blend phases, and reactive compatibilization has been recognized as an effective method for producing blends [2, 55, 56].

Glycidyl methacrylate (GMA) grafted copolymers were usually used to toughen plastics [57–59]. In this study, ethylene-methyl-acrylate-glycidyl methacrylate copolymer (EMA-GMA) was selected to act as a compatibilizer for POM/EBA blends. EMA has a good compatibility with EBA, because they are both ethylene-acrylic esters with similar chain structures. Conversely, and as shown in Fig. 1, epoxy functional groups of EMA-GMA can react with terminal hydroxyl groups of POM to generate a new graft copolymer [60–62] at the interface that enhances the compatibility by reducing the interfacial tension between the blend components.

*Correspondence to*: X.-L. Wang; e-mail: wangxuanlun@cqut.edu.cn or Z. Guo; e-mail: zguo10@utk.edu
Contract grant sponsor: Chongqing Municipal Key Laboratory of Institutions of Higher Education for Mould Technology; contract grant number: MT201507.
DOI 10.1002/pen.24675
Published online in Wiley Online Library (wileyonlinelibrary.com).

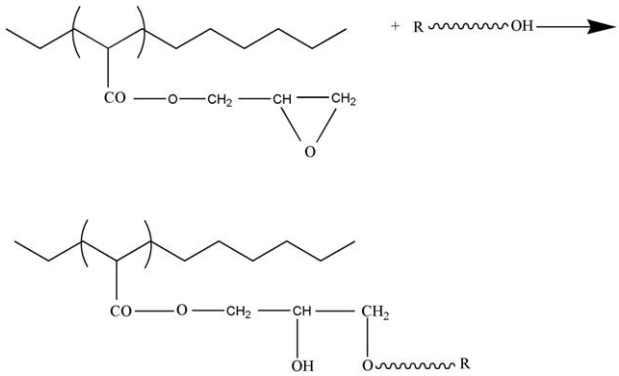

FIG. 1. Reaction scheme between POM and EMA-GMA.

The toughening effect of EBA to POM with various ratios will be investigated in this work. The mechanical properties, dynamic rheological behavior, dynamic mechanics performance, thermo-gravimetric analysis (TGA), and morphology of both the uncompatibilized POM/EBA blends and compatibilized POM/EBA/EMA-GMA blends were investigated to demonstrate the necessity of the compatibilizer.

## EXPERIMENTAL

### *Materials*

POM copolymer (commercial grade, M90) was purchased from Yuntianhua Company, China. Its melt flow rate (190°C, 2.16 kg) was 9 g/10min and its density was 1.41 g/cm$^3$. The toughening agent EBA (3117AC) was purchased from DuPont, America. Its melt flow rate (190°C, 2.16 kg) was 1.5 g/10min, and its content of butylacrylate was 17 wt%. EMA-GMA (AX8900, $M_w$: 2 $\times 10^5$, GMA grafting ratio is 8%) was obtained from Arkema, France.

### *Blends Preparation*

The compatibilized POM/EBA/EMA-GMA blends and uncompatibilized POM/EBA blends with different component ratios were prepared by two-step method, EBA and EMA-GMA were blended first by weight ratio 2:1 to make masterbatch, then the masterbatch was used to blend with POM. Codes of the blends were E-5 (POM/EBA/EMA-GMA:95/5/2.5), E-15 (POM/EBA/EMA-GMA:85/15/7.5), E-5* (POM/EBA:95/5), E-15* (POM/EBA:85/15), the ratios in the sample codes were calculated by weight.

The POM copolymer was dried at 80°C in a fan blower type electric drying oven (Blue Pard, BPG-9070A, China) for 3 h. The EBA and EMA-GMA were dried at 50°C for 3 h. Then different components were blended in a co-rotating twin-screw extruder (TSE-30A, L/D: 40:1, Nanjing Ruiya Polymer Processing Equipment Company, China). The extrusion temperatures at different zones from the feeding hopper to the extrusion die were 115°C, 130°C, 170°C, 190°C, 195°C, 195°C, 195°C, 195°C, 195°C, 195°C, and 190°C respectively, and the screw speed was 200 rpm. Before injection molding, the moist granules were dried enough to remove the water from the granules. The injection molding process was operated by an injection molding machine (EM80-SVP/2, ZhenXiong Co., Taiwan), and temperatures from feed aperture section to nozzle was 20°C, 165°C, 185°C, 190°C, and 185°C, respectively, injecting pressure was 120 MPa. The mould was with two-cavity, a standard dumbbell-shaped sample for tensile test and a rectangle sample (80 mm $\times$10 mm $\times$ 4 mm) were obtained. And then a notching machine (XQZ-1, Chengde Jinjian Testing Instrument Company, China) was used to make a B-type notched samples (the depth was 2 mm) with the rectangle samples for the impact strength test.

### *Mechanical Performance Testing*

The tensile test was operated by a microcomputer controlled universal tensile testing machine (CMT 6104, MTS systems (China) Co., Ltd.) according to GB/T 1040–92 at the test speed of 20 mm/min.

The notched Izod impact strength tests were conducted by a pendulum impact testing machine (ZBC1400-B, MTS systems Co., Ltd, China) according to GB/T 1843–1996. Either for the tensile test, or for the impact test, at least five samples were prepared every time. Dumbbell samples were used for tensile test and rectangular samples were for Izod impact test. All the tensile tests and impact tests were carried in an environment of 25°C constant temperature. The mechanical results calculated as a function of the original cross-section.

### *Infrared Spectroscopic Analysis*

EMA-GMA were compression molded into thin films by a molding press (BL6170-A, Bolon Precision Testing Machines, Co., Ltd, China), neat POM and E-15 were solved by hexafluoroisopropanol, after the volatilization of hexafluoroisopropanol, thin films of neat POM and E-15 were obtained respectively. Then, the thin films of the three samples were used for FTIR characterization in a Fourier transform infrared Spectrum instrument (Nicolet$^{TM}$ iS$^{TM}$10, Thermo Fisher, America).

### *Dynamic Rheological Measurement*

Dynamic rheological behavior of different samples was tested by a rotational rheometer (AR-1500ex, TA Instruments). Steel plate diameter was 25 mm, and the testing gap was 1 mm. The testing mode was frequency sweep, the frequency was varied from 0.01 to 100 Hz, the testing temperature was 185°C, and the strain was 3% to fall within the linear viscoelastic region.

### *Dynamic Mechanical Performance*

Dynamic Mechanical performance of different samples were assessed by a dynamic mechanical analyzer (DMA Q800, TA Instruments). The testing mode was DMA Multi-Frequency-Strain, the testing frequency was 10 Hz (single frequency), the sample sizes were about 35 mm $\times$ 10 mm $\times$ 4 mm. The samples were obtained by cutting the injected samples (80 mm $\times$ 10 mm $\times$ 4 mm). The testing temperature range for POM, POM/EBA blends and POM/EBA/EMA-GMA blends were from $-$75°C to 165°C. The testing temperature range for EBA and EMA-GMA were from $-$75°C to 56°C. The heating rate was 3°C/min.

 DOI 10.1002/pen

TABLE 1. Mechanical properties of samples (/standard deviation values).

| Sample | $\sigma_M$[a] | $\varepsilon_B$[b] | $E$[c] | Izod[d] |
|---|---|---|---|---|
| POM | 60.34/0.97 | 34/0.54 | 2635/52.71 | 16.36/0.33 |
| E-5 | 49.85/0.59 | 38/0.46 | 2133/45.31 | 22.16/0.31 |
| E-15 | 37.91/0.57 | 47.94/0.67 | 1517/36.41 | 20.71/0.31 |
| E-5* | 48.35/0.73 | 37.05/0.56 | 2056/43.18 | 19.98/0.30 |
| E-15* | 36.84/0.74 | 45.85/0.59 | 1465/33.71 | 17.31/0.28 |
| EBA | 8.31/0.15 | 286.93/5.76 | 25.88/0.36 | — |
| EMA-GMA | 3.83/0.08 | 786.95/6.09 | 4.4/0.06 | — |

[a]Tensile strength (MPa).
[b]Elongation at break (%).
[c]$E$ is tensile modulus (MPa).
[d]Notched izod impact strength (kJ/m$^2$).

*Thermo-Gravimetric Analysis*

Thermal degradation behavior of the samples was conducted by a TGA analyzer (Q50, TA Instruments). The tests were performed under nitrogen atmosphere with a nitrogen flow rate of 60 mL/min. The samples were heated from 25 to 600°C at 10°C/min.

*The Microstructure Analysis*

The microstructure photos of the samples were obtained by a scanning electron microscope (SEM, JSM-6460LV, JEOL, Japan). The notched impact fracture surfaces of different samples were sputtered coated with gold before SEM observations.

## RESULTS AND DISCUSSION

*Mechanical Properties*

The mechanical properties of the raw materials and the uncompatibilized (POM/EBA) and compatibilized (POM/EBA/EMA-GMA) blends are shown in Table 1. Obviously, E-5 had a maximum notched impact strength of 22.16 kJ/m$^2$, which was 35.45% higher than that of pure POM (16.36 kJ/m$^2$). When pure POM was subjected to an impact, the crack expanded from the notch, so pure POM fractured. For the blends, the energy passed from POM matrix to EBA particles via interface. The EBA particles would absorb impact energy by elongation transformation as its elongation at break was as high as 286.93%, and thus the impact strength of the blends improved. As observed on SEM pictures shown later, E-5 exhibited a "wave-shaped" rough fracture surface, indicating a ductile fracture. While other samples got relatively smooth fracture surface. With more EBA added, the notched impact strength declined gradually. The toughness of the POM was improved obviously with a relatively low adding of EBA. According to SEM photos, with increasing the EBA loading, the dispersed phase agglomerated, and the sizes of dispersed phase increased, thus the interfacial area between these two phases decreased. The EBA particles absorbed less energy through the interface during deformation.

Generally, toughening brittle polymers by blending with ductile polymers always resulted in a reduced tensile strength [18]. The tensile strength gradually declined from 60.34 for pure POM to 37.91 MPa for the compatibilized blends (E-15). As EBA is a ductile plastic, the elongation at break of POM/EBA/EMA-GMA increased with increasing the EBA loading continually. In a blend system, the addition of low modulus materials always resulted in lower modulus of the blend system [44]. In the compatibilized blends system, EBA had a much lower modulus compared to POM. Thus, with more EBA added, the modulus of the blends declined gradually from 2,635 for pristine POM to 1,517 MPa for (E-15).

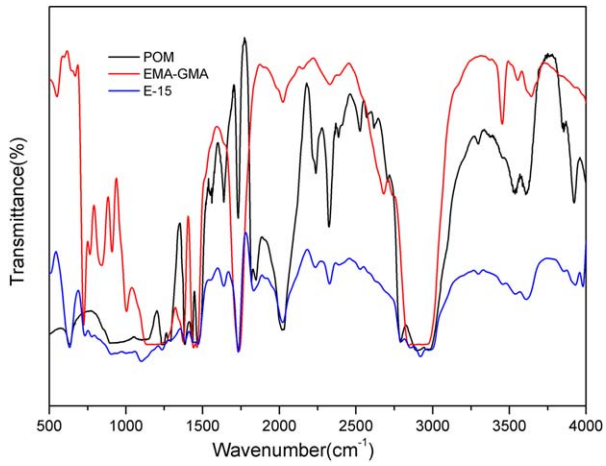


FIG. 2. FTIR spectra of pure POM, E-15, and EMA-GMA. [Color figure can be viewed at wileyonlinelibrary.com]

In addition, to verify the compatibilization effect of EMA-GMA, the uncompatibilized POM/EBA blends were tested. The uncompatibilized POM/EBA blends also had a higher notched impact strength than pure POM, as EBA is an excellent toughening agent with high molecular polarity that matches that of POM. The notched impact strength also decreased from E-5* to E-15* due to the agglomeration of EBA particles. In addition, due to the absence of EMA-GMA compatibilizer, the uncompatibilized blends had a little lower notched impact strength than their compatibilized counterparts, as the epoxy functional groups from EMA-GMA reacted with the terminal hydroxyl groups from POM, and formed a new graft copolymer. EMA had a similar molecular structure to EBA, thus POM matrix and EBA particles had a stronger interfacial adhesion than the uncompatibilized blends. The compatibilized POM/EBA/EMA-GMA blends had a higher notched impact strength than their uncompatibilized counterparts. Including the notched impact strength, the uncompatibilized POM/EBA blends with a lower interfacial adhesion had worse properties than the compatibilized POM/EBA/EMA-GMA blends, such as tensile strength, elongation at break, and tensile modulus, as listed in Table 1.

*Infrared Spectroscopic Analysis*

Figure 2 shows the FTIR spectra of neat POM EMA-GMA and E-15. EMA-GMA had epoxy groups, and the absorbance of epoxy groups was at 911 and 844 cm$^{-1}$ [61]. Conversely, E-15 had no absorbance of epoxy groups. This phenomenon indicated that the absorbance of epoxy groups of EMA-GMA reacted with terminal hydroxyl groups of POM molecular chains. Figure 1 shows the reaction scheme between the molecules of POM and EMA-GMA [60–62].

New grafted copolymer was generated. In this reaction, primary hydroxyl groups of POM reacted with epoxy groups of EMA-GMA, generating secondary hydroxyl groups. Both the primary and secondary hydroxyl groups had absorbance at about

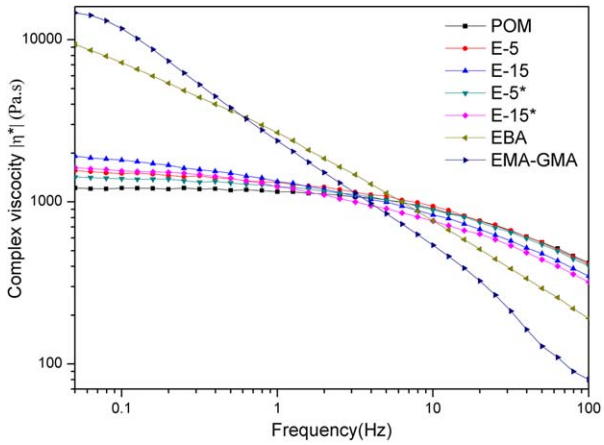


FIG. 3. Complex viscosity versus frequency of the raw materials and their blends. [Color figure can be viewed at wileyonlinelibrary.com]

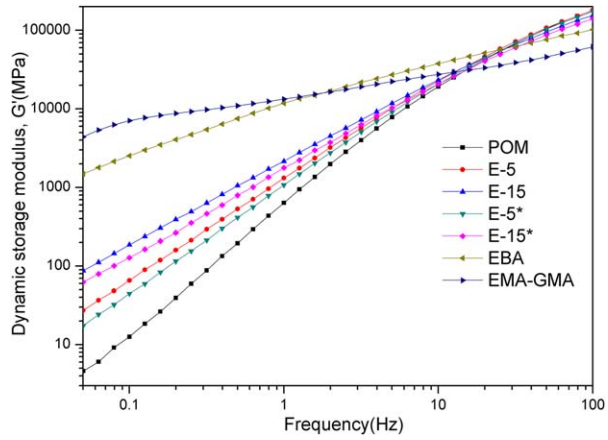


FIG. 4. Dynamic storage modulus versus frequency of the raw materials and their blends. [Color figure can be viewed at wileyonlinelibrary.com]

3,303 $cm^{-1}$, confirming that the absorbance at 3,303 $cm^{-1}$ in E-15 FTIR spectrum was the secondary hydroxyl groups generated by the reaction. Thus, the EMA-GMA was proved to be reactive compatibilizer in the POM/EBA/EMA-GMA blends, and had a good compatibility with POM.

*Dynamic Rheological Behavior*

Figure 3 shows the change of complex viscosity versus frequency of the raw materials and the uncompatibilized (POM/EBA) and compatibilized (POM/EBA/EMA-GMA) blends. The complex viscosity of all the samples decreased with increasing the frequency. This was due to the strong shear thinning behavior of the POM/EBA blends and their pure components at the melting state. Obviously, at low frequency region, the complex viscosity of EBA and EMA-GMA was much higher than that of POM and the blends. For the POM/EBA compatibilized systems, the complex viscosity increased with increasing the content of EBA and EMA-GMA, Table 2. This was not only attributed to the strong interaction between the POM matrix and EBA particles in the presence of the compatibilizer EMA-GMA but also because two highly viscous rubbers EBA and EMA-GMA were added to a low viscous POM material. In the compatibilized blends, the compatibilizer molecular chains are linked to the interface and form strong interactions between these two phases, thus the interfacial adhesion strength was increased [63]. The compatibilizer resulted in an effective stress transfer between the POM matrix and high viscosity EBA particles, thus the interlayer slippage ability was reduced, and the viscosity of the blends increased with increasing the EBA and compatibilizer content.

TABLE 2. Dynamic rheological properties of the samples (at 0.1 Hz).

| Sample | $G'$(Pa) | $G''$(Pa) | $\lvert\eta^*\rvert$(Pa s) |
|---|---|---|---|
| POM | 12.54 | 764.2 | 1216 |
| E-5 | 65.68 | 938.9 | 1498 |
| E-15 | 186.3 | 1124 | 1813 |
| E-5* | 44.5 | 871.3 | 1389 |
| E-15* | 127.5 | 965.1 | 1549 |
| EBA | 2537 | 3765 | 7226 |
| EMA-GMA | 7080 | 2070 | 11740 |

Exactly the same trend as for the compatibilized system was noticed, that is, the complex viscosity of all the samples in the compatibilized system decreased with increasing the frequency because of the strong shear thinning behavior at the melting state. The complex viscosity increased with increasing the content of EBA at low frequency region, Table 2. Due to the absence of compatibilizer, the interface adhesion was not as strong as in the compatibilized systems; thus, the complex viscosity of the uncompatibilized POM/EBA blends was lower than that of the compatible counterparts, Table 2. For instance, E-5* showed a lower complex viscosity than that of E-5. At 0.1 Hz, the complex viscosity of E-5* was 1,389 Pa.s, 7.3% lower than that of E-5, because of the weaker interaction between POM matrix and EBA particles in the uncompatibilized blend E-5*.

In the high frequency region, the complex viscosity of EBA was lower than that of POM and POM/EBA blends, indicating that EBA possessed stronger shear thinning behavior than POM. The change of $G'$ (storage modulus) and $G''$ (loss modulus) according to the frequency of the compatibilized and uncompatibilized systems and their pristine components are exhibited in Figure 4 and Figure 5, respectively. For all the samples in both the uncompatibilized and compatibilized systems, both $G'$ and $G''$ increased with increasing the frequency. In the low frequency region, the time was sufficient for the molecular

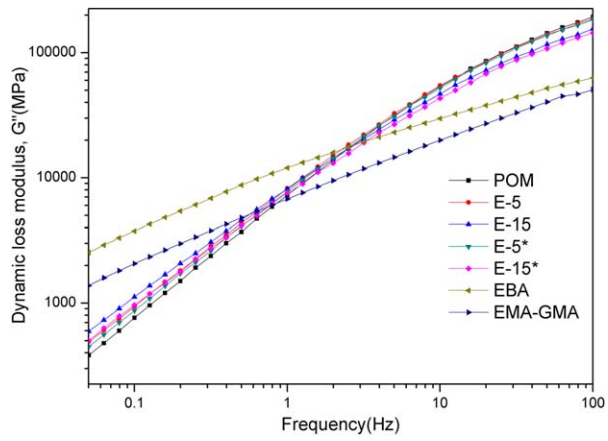


FIG. 5. Dynamic loss modulus versus frequency of the raw materials and their blends. [Color figure can be viewed at wileyonlinelibrary.com]


DOI 10.1002/pen

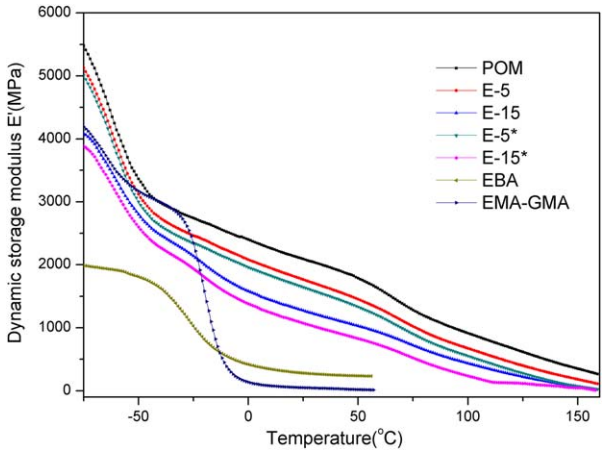


FIG. 6. Dynamic storage modulus versus temperature of the raw materials and their blends. [Color figure can be viewed at wileyonlinelibrary.com]

entanglements to unfasten, hence a number of relaxation took place, thus $G'$ and $G''$ were low. While in the high frequency region, the molecular entanglements required very shorter time to relax, thus both $G'$ and $G''$ became higher [18]. In the low frequency region, EBA and EMA-GMA had much higher $G'$ and $G''$ than those of POM and POM/EBA blends. In both compatibilized and uncompatibilized systems, both $G'$ and $G''$ of the samples increased with increasing the content of EBA and EMA-GMA. In addition, for both $G'$ and $G''$, the values of the compatibilized blends were higher than those of their uncompatibilized counterparts, Table 2. For instance, E-5 had higher $G'$ and $G''$ than E-5*. The POM matrix had a stronger interaction with EBA particles through the interface in the presence of compatibilizer EMA-GMA, while the interface in the incompatible blends was weaker in the absence of EMA-GMA, thus EMA-GMA was proved to be a good compatibilizer for the POM/EBA blends. Thus, for the storage modulus $G'$ and loss modulus $G''$, the reasons for the observed changes are not only due to the reaction between EMA-GMA and POM but also due to the fact that a great part of a solid like materials that is POM with two rubbers are changed. In the high frequency region, both $G'$ and $G''$ values of EBA and EMA-GMA became lower than those of POM and the blends. And for both the compatibilized and uncompatibilized blends, the tendency is that with more EBA and EMA-GMA blended with POM, the $G'$ and $G''$ values became lower.

*Dynamic Mechanical Analysis*

Figure 6 shows the change of dynamic storage modulus ($E'$) as a function of temperature of the raw materials and the uncompatibilized (POM/EBA) and compatibilized (POM/EBA/EMA-GMA) blends. Obviously, POM had a much higher storage modulus than EBA at any temperature. The storage modulus has a positive correlation with stiffness [64]. This corresponds to the fact that POM is a stiff material and EBA is a soft toughening plastic agent. As to the POM/EBA/EMA-GMA blends, the $E'$ values of the blends were lower than that of pure POM, and the $E'$ decreased with increasing the content of EBA. The $E'$ of POM and its blends started decreasing rapidly at −75°C and the decrease slowed down at −60°C, for EBA, the rapid decrease stated at around −40°C and the decrease slowed down at −18°C, and the $E'$ of EMA-GMA started decreasing rapidly at around −75°C and the decrease slowed down at −60°C, then it decreased rapidly at around −25°C and the decrease slowed down at −10°C. In addition, the compatibilized POM/EBA/EMA-GMA blends had higher modulus than the uncompatibilized counterparts. Figure 9 and Table 4 show that the particles distribution in the compatibilized system is more uniform than the particles distribution in the uncompatibilized system. This indicated that compatibilizer EMA-GMA existed in the interface between POM and EBA, thus the agglomeration in the compatibilized system was weakened. So the existence of EBA in the interface between POM and EBA increased the interface thickness and thus the interfacial adhesion between POM matrix and EBA particles increased, to increase the stress transfer between the interfaces.

Figure 7 shows the change of loss modulus versus temperature of the raw materials and the uncompatibilized (POM/EBA) and compatibilized (POM/EBA/EMA-GMA) blends. Apparently, POM exhibited two evident relaxation peaks at about 120°C (α) and −62.52°C (γ), respectively. The α relaxation corresponded to the segment motion in the crystals, which was due to the reorientation of defect areas in the crystalline phase [65]. The β

TABLE 3. The onset degradation temperatures of the samples.

| Sample | $T_d$ (°C) |
|---|---|
| POM | 335.24 |
| E-5 | 345.74 |
| E-15 | 350.36 |
| E-5* | 340.79 |
| E-15* | 348.35 |
| EBA | 402.86 |
| EMA-GMA | 388.48 |

TABLE 4. EBA particle size distribution in POM matrix of the blends.

| | Sample | | | |
|---|---|---|---|---|
| Test item | E-5 | E-15 | E-5* | E-15* |
| Particle numbers | 276 | 250 | 266 | 200 |
| Average diameter (μm) | 1.36 | 2.13 | 1.53 | 2.35 |

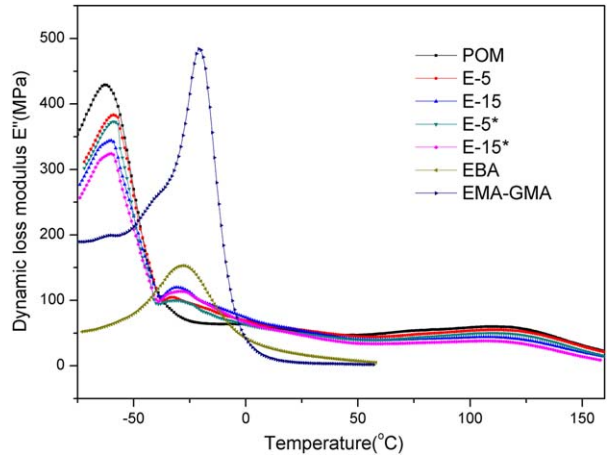


FIG. 7. Loss modulus versus temperature of the raw materials and their blends. [Color figure can be viewed at wileyonlinelibrary.com]

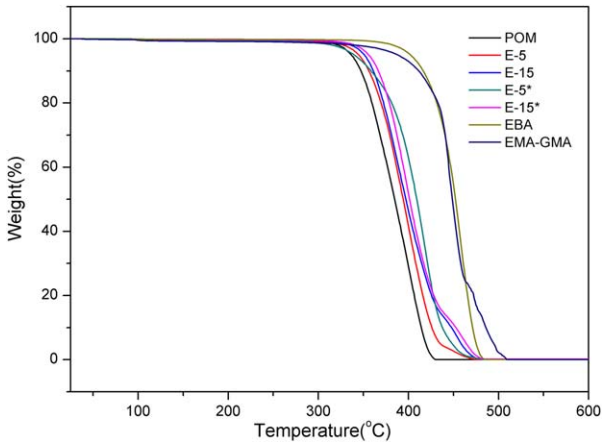


FIG. 8. TGA thermograms of the raw materials and their blends. [Color figure can be viewed at wileyonlinelibrary.com]

relaxation of POM was not evident, due to the lack of branched chains. The $\gamma$ relaxation corresponded to the segment motion in the amorphous regions, the glass-transition temperature ($T_g$) was selected as the peak position of dynamic loss modulus when plotted as a function of temperature [66]. Thus, in this article, the $\gamma$ relaxation peak was identified as the $T_g$. There was a single relaxation observed in the EBA dynamic loss modulus curve. The peak value of the relaxation peak was identified as the $T_g$ of EBA. In addition, three relaxation regions were identified in the POM/EBA/EMA-GMA blends. The peak values at about $-60$ and $-30$°C corresponded to the $T_g$ values of POM phase and EBA phase, respectively. Obviously, the $T_g$ values of the POM phase in the compatibilized blends were a little higher than that of pure POM, while the $T_g$ values of the EBA phase in the compatibilized blends were a little lower than that of EBA. Namely, the $T_g$ values of the components in the blends shifted to each other, this was the most distinct evidence of the occurrence of compatibility between these two components.

The $T_g$ values of the components also shifted to each other in the uncompatibilized POM/EBA blends, this proved that pure POM and EBA had a compatibility to a certain extent. Conversely, the range of $T_g$ of POM and EBA shifted to each other in the compatibilized blends and was larger than the uncompatibilized blends. This proved that the compatibilizer EMA-GMA improved the compatibility between POM and EBA. According to Fig. 7, the $T_g$ shift range of POM and EBA decreased with increasing the content of EBA in the investigated blends for both the compatibilized (from E-5 to E-15) and uncompatibilized blends (from E-5* to E-15*). When the content of EBA increased, the EBA particles agglomerated and the size of particles increased, Fig. 9, thus the interface area decreased.

*Thermal Stability*

Figure 8 shows the TGA curves of the raw materials and the uncompatibilized POM/EBA and compatibilized POM/EBA/EMA-GMA blends. The onset of degradation temperatures of the samples was determined by plotting tangent with the curves where the weight began to decline. Both EBA and POM showed a single stage of thermal degradation, while the blends showed two stages behavior. Apparently, pure POM had the lowest onset degradation temperature, because POM is thermally unstable, this is well known and mainly due to the presence of

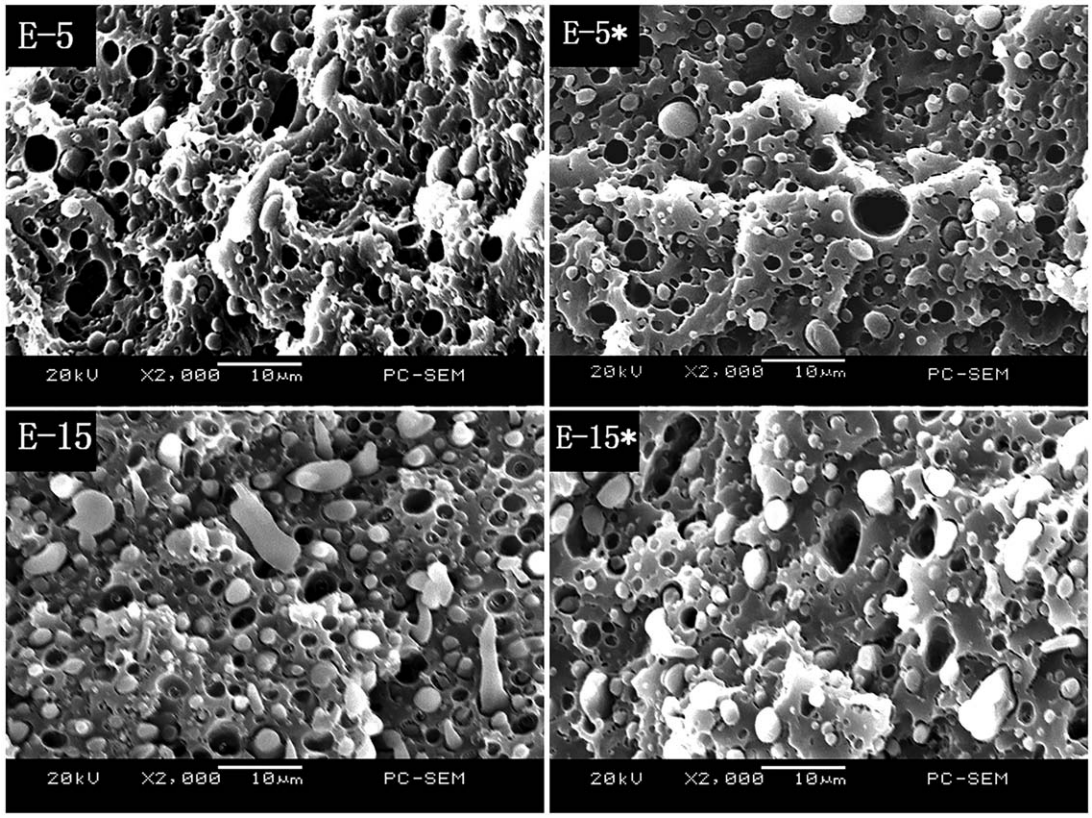


FIG. 9. SEM microscopic photos of the compatibilized and uncompatibilized blends.


DOI 10.1002/pen

—O—$CH_2$—OH end groups leading to a mechanism of "unzipping." In addition, the onset degradation temperature of the compatibilized blends increased with increasing the content of EBA and EMA-GMA, as they had much higher thermal stability than POM. Conversely, the onset degradation temperature of POM/EBA blends was also between those of pure POM and EBA, and the onset degradation temperature of the uncompatibilized blends also increased with increasing the content of EBA as it had much higher thermal stability than POM, Table 3. This might be because the more dispersed EBA particles absorbed more heat, thus delayed the thermal degradation of POM matrix. With more EBA added into the blends, more heat was absorbed by the EBA particles, thus the onset degradation temperature of the blends increased. In addition, the onset degradation temperatures of the compatibilized blends were a little higher than that of their uncompatibilized counterparts. This is due to the addition EMA-GMA that had a synergistic effect with EBA and also due to the higher stability of EMA-GMA compared to POM.

*Microstructure Analysis*

Figure 9 shows the microstructures of the compatibilized and uncompatibilized blends. The EBA particles distribution in the POM matrix with and without compatibilizer are shown in Table 4. In the compatibilized POM/EBA/EMA-GMA blends, with the content of EBA increased, the agglomeration became more and more obvious, the size of EBA particles increased. The notched impact fracture surface of E-5 was rough, indicating that E-5 was ductile fractured, while the notched impact fracture surfaces of other blends were relatively smooth, indicating that the other blends were brittle fractured. This was because from sample E-5 to sample E-15, when more EBA was added, the agglomeration became more pronounced, the size of EBA particles increased, and the interfacial area between the POM matrix and EBA particles decreased. The EBA particles absorbed less energy through the interface by deformation, thus the notched impact strength decreased. Conversely, in the case of POM/EBA uncompatibilized blends, their notched impact strength decreased with increasing the EBA content for the same reason with the compatibilized blends. In addition, due to the absence of compatibilizer, the EBA could not be uniformly dispersed, the agglomeration became even worse. The SEM photos show that the sizes of uncompatibilized blends were more irregular than their compatibilized counterparts. For the uncompatibilized blends, the particle size increased and the particle size distribution was broadened with increasing the content of dispersed phase due to the increased agglomeration [50]. In addition, the effect of compatibilizer in the polymer blends was to restrict the agglomeration by stabilizing the interface, through reduction of the interfacial tension. Thus, the notched impact strength of the uncompatibilized blends was a little lower than that of their compatibilized counterparts. This also demonstrated the necessity of adding EMA-GMA compatibilizer to POM/EBA blends.

## CONCLUSIONS

Uncompatibilized POM/EBA blends had a higher notched impact strength than pure POM, and the compatibilized POM/EBA/EMA-GMA had a higher notched impact strength than their uncompatibilized counterparts. The toughness of the POM was improved obviously with relatively low adding of EBA. FTIR spectra showed that the epoxy groups of EMA-GMA reacted with terminal hydroxyl groups of POM molecular chains in the POM/EBA/EMA-GMA blends. Dynamic rheological behavior showed that, at low frequency region, for both the uncompatibilized POM/EBA blends and compatibilized POM/EBA/EMA-GMA blends, the $|\eta^*|$, $G'$ and $G''$ of the blends all increased with increasing the content of EBA, and the uncompatibilized blends values were lower than their compatibilized counterparts. Dynamic mechanical analysis showed that, for both the uncompatibilized POM/EBA blends and compatibilized POM/EBA/EMA-GMA blends, the storage modulus and loss modulus both decreased with increasing the content of EBA. The glass transition temperature values of compatibilized blends were higher than that of their uncompatibilized counterparts. POM and EBA had compatibility to a certain extent, and the compatibilizer increased the compatibility between these two phases. TGA indicated that both the uncompatibilized POM/EBA blends and the compatibilized POM/EBA/EMA-GMA blends had better thermal stability than pure POM. The microstructure observation showed that the POM/EBA/EMA-GMA blend exhibited obvious rough impact fracture surface, indicating that the samples were ductile fractured, while other uncompatibilized blends exhibited smooth impact fracture surface. The effect of compatibilizer in the polymer blends was to restrict the agglomeration by stabilizing the interface, through the reduction of interfacial tension. In the uncompatibilized system, agglomeration became more serious, the interfacial area between the POM matrix and EBA particles decreased, EBA particles absorbed less energy through the interface by deformation.

## REFERENCES


1. C. Wang, Y. Wu, Y. Li, Q. Shao, X. Yan, C. Han, Z. Wang, Z. Liu, and Z. Guo, *Polymers for Advanced Technologies*, in press, doi: 10.1002/pat.4105
2. V.J. Triacca, S. Ziaee, J.W. Barlow, H. Keskkula, and D.R. Paul, *Polymer*, **32**, 1401 (1991).
3. B. Majumdar, H. Keskkula, and D.R. Paul, *Polymer*, **35**, 3164 (1994).
4. G. Li, V. Shrotriya, J. Huang, Y. Yao, T. Moriarty, K. Emery, and Y. Yang, *Nat. Mater.*, **4**, 864 (2005).
5. S. Wu, *Polymer*, **26**, 1855 (1985).
6. L.A. Utracki and B.D. Favis, *Polymer Alloys and Blends, Vol. 4*. Marcel Dekker, New York (1989).
7. C. Koning, M. Van Duin, C. Pagnoulle, and R. Jerome, *Prog. Polym. Sci.*, **23**, 707 (1998).
8. D.R. Paul, *Polymer Blends*, Elsevier Publisher, Amsterdam, Netherlands, 2012.
9. L. Yu, K. Dean, and L. Li, *Prog. Polym. Sci.*, **31**, 576 (2006).
10. Y. Li, X. Wu, J. Song, J. Li, Q. Shao, N. Cao, N. Lu, and Z. Guo, *Polymer*, in press, doi: 10.1016/j.polymer.2017.07.042.
11. J. Gu, W. Dong, Y. Tang, Y. Guo, L. Tang, J. Kong, S. Tadakamalla, B. Wang, and Z. Guo, *J. Mater. Chem. C*, in press, doi:10.1039/C7TC00222J
12. Z. Sun, L. Zhang, F. Dang, Y. Liu, Z. Fei, Q. Shao, H. Lin, J. Guo, L. Xiang, N. Yerra, and Z. Guo, *CrystEngComm*, **19**, 3288 (2017).
13. J. Gu, X. Meng, Y. Tang, Y. Li, Q. Zhuang, and J. Kong, *Compos. Part A: Appl. Sci. Manuf.*, **92**, 27 (2017).

14. J. Gu, Z. Lv, Y. Wu, Y. Guo, L. Tian, H. Qiu, W. Li, and Q. Zhang, *Compos. Part A: Appl. Sci. Manuf.*, **94**, 209 (2017).
15. Y. Zheng, Y. Zheng, S. Yang, Z. Guo, T .Zhang, H. Song, and Q. Shao, *Green Chem. Lett. Rev.*, **10**, 202 (2017).
16. S. Bagheri-Kazemabad, D. Fox, Y. Chen, L.M. Geever, A. Khavandi, R. Bagheri, and B. Chen, *Compos. Sci. Technol.*, **72**, 1697 (2012).
17. L. Li, B. Yin, Y. Zhou, L. Gong, M. Yang, B. Xie, and C. Chen, *Polymer*, **53**, 3043 (2012).
18. L. Ma, X. Wei, Q. Zhang, W. Wang, L. Gu, W. Yang, and M. Yang, *Mater. Des.*, **33**, 104 (2012).
19. C. Papadopoulou and N. Kalfoglou, *Polymer*, **41**, 2543 (2000).
20. N. Kalfoglou, D. Skafidas, J. Kallitsis, J. Lambert, and L. Van der Stappen, *Polymer*, **36**, 4453 (1995).
21. B. Lombardo, H. Keskkula, and D. Paul, *J. Appl. Polym. Sci.*, **54**, 1697 (1994).
22. A. Stephan, Y. Saito, N. Muniyandi, N. Renganathan, S. Kalyanasundaram, and R. Elizabeth, *Solid State Ionics*, **148**, 467 (2002).
23. C.E. Carraher, *Giant Molecules: Essential Materials for Everyday Living and Problem Solving*, John Wiley & Sons, Hoboken, New Jersey, USA (2003).
24. Q. Zhong and F. Chen, *CAAI Trans. Intell. Technol.*, **1**, 197 (2016).
25. X. Zhang, H. Gao, M. Guo, G. Li, Y. Liu, and D. Li, *CAAI Trans. Intell. Technol.*, **1**, 4 (2016).
26. C. Alippi, *CAAI Trans. Intell. Technol.*, **1**, 1 (2016).
27. Y. Lan, H. Liu, and X. Cao, *Polymer*, **97**, 11 (2016).
28. K. Palanivelu, P. Sivaraman, and M.D. Reddy, *Polym. Test.*, **21**, 345 (2002).
29. F. Feng and L. Ye, *J. Appl. Polym. Sci.*, **119**, 2778 (2011).
30. J. Han and H. Huang, *J. Appl. Polym. Sci.*, **120**, 3217 (2011).
31. P. Poomalai and P. Piddaramaiah, *J. Macromol. Sci. Part A: Pure Appl. Chem.*, **42**, 1399 (2005).
32. F. Chang and M.Y. Yang, *Polym. Eng. Sci.*, **30**, 543 (1990).
33. K. Palanivelu, S. Balakrishnan, and P. Rengasamy, *Polym. Test.*, **19**, 75 (2000).
34. G. Kumar, N. Neelakantan, and N. Subramanian, *J. Mater. Sci.*, **30**, 1480 (1995).
35. G. Kumar, N.R. Neelakantan, and N. Subramanian, *Polym. Plast. Technol. Eng.*, **32**, 33 (1993).
36. X. Gao, C. Qu, and Q. Fu, *Polym. Int.*, **53**, 1666 (2004).
37. G. Kumar, M.R. Arindam, N.R. Neelakantan, and N. Subramanian, *J. Appl. Polym. Sci.*, **50**, 2209 (1993).
38. M. Mehrabzadeh and D. Rezaie, *J. Appl. Polym. Sci.*, **84**, 2573 (2002).
39. W. Tang, H. Wang, J. Tang, and H. Yuan, *J. Appl. Polym. Sci.*, **127**, 3033 (2013).
40. E.A. Flexman, Jr., U.S. Patent 5,318,813 (1994).
41. K. Pielichowski and A. Leszczynska, *J. Polym. Eng.*, **25**, 359 (2005).
42. R. Uthaman, A. Pandurangan, and S. Majeed, *Polym. Eng. Sci.*, **47**, 934 (2007).
43. A. Grigalovica, R. Meri, J. Zicans, T. Ivanova, and J. Grabis, *IOP Conf. Ser.: Mater. Sci. Eng.* **49**, 12004 (2013).
44. R. Uthaman, A. Pandurangan, and S. Majeed, *J. Polym. Res.*, **14**, 441 (2007).
45. X. Ren, L. Chen, H. Zhao, Y. Dan, and X. Cai, *J. Macromol. Sci., Part B: Phys.*, **46**, 411 (2007).
46. Y. Liu, T. Zhou, Z. Chen, L. Li, Y. Zhan, A. Zhang, and F. Liu, *Polym. Adv. Technol.*, **25**, 760 (2014).
47. Y. Gao, S. Sun, Y. He, X. Wang, and D. Wu, *Compos. B: Eng.*, **42**, 1945 (2011).
48. G. Balamurugan and S. Maiti, *Eur. Polym. J.*, **43**, 1786 (2007).
49. H. Liu, L. Guo, X. Guo, and J. Zhang, *Polymer*, **53**, 272 (2012).
50. U. Sundararaj and C.W. Macosko, *Macromolecules*, **28**, 2647 (1995).
51. L. Minkova, H. Yordanov, and S. Filippi, *Polymer*, **43**, 6195 (2002).
52. R.A. Kudva, H. Keskkula, and D.R. Paul, *Polymer*, **41**, 239 (2000).
53. Y. Wang, Q. Zhang, and Q. Fu, *Macromol. Rapid Commun.*, **24**, 231 (2003).
54. D. Bikiaris and C. Panayiotou, *J. Appl. Polym. Sci.*, **70**, 1503 (1998).
55. M. Xanthos and S. Dagli, *Poly. Eng. Sci.*, **31**, 929 (1991).
56. L. Wang, W. Ma, R.A. Gross, and S.P. McCarthy, *Polym. Degrad. Stab.*, **59**, 161 (1998).
57. E. Lievana and J. Karger-Kocsis, *Macromol. Symp.* **202**, 59 (2003).
58. D.E. Mouzakis, N. Papke, and J. Wu, *J. Appl. Polym. Sci.*, **79**, 842 (2001).
59. N. Papke and J. Karger-Kocsis, *Polymer*, **42**, 1109 (2001).
60. W. Hale, H. Keskkula, and D.R. Paul, *Polymer*, **40**, 365 (1999).
61. P. Martin, J. Devaux, J. Legras, R. Van Gurp, and M. Van Duin, *Polymer*, **42**, 2463 (2001).
62. W. Yang, X.L. Wang, X. Yan, and Z. Guo, *Polym. Eng. Sci.*, in press. doi:10.1002/pen.24489
63. P. Ezzati, I. Ghasemi, M. Karrabi, and H. Azizi, *Iran. Polym. J.*, **17**, 669 (2008).
64. Dynamic Mechanical Analyzer, Q Series™, Getting started guide, Revision F, TA Instruments, Cincinnati, Ohio, USA (2004).
65. S. Mohanty, S. Verma, and S. Nayak, *Compos. Sci. Technol.*, **66**, 538 (2006).
66. C. Komalan, K. George, P.A. Kumar, K.T. Varughese, and S. Thomas, *Express Polym. Lett.*, **1**, 641 (2007).

 DOI 10.1002/pen